HHS Public Access

Author manuscript

Nat Neurosci. Author manuscript; available in PMC 2013 September 09.

Published in final edited form as:

Nat Neurosci. 2011 February ; 14(2): 224–231. doi:10.1038/nn.2707.

Thalamic interneurons and relay cells use complementary synaptic mechanisms for visual processing

Xin Wang[1,*], **Vishal Vaingankar**[1], **Cristina Soto Sanchez**[1], **Friedrich T. Sommer**[2], and **Judith. A. Hirsch**[1]

[1]Department of Biological Sciences and Neuroscience Graduate Program, University of Southern California, 3641 Watt Way, Los Angeles, CA 90089-2520, USA

[2]Redwood Center for Theoretical Neuroscience, University of California, Berkeley, 132 Barker, Berkeley, CA 94720-3190, USA

Abstract

Synapses made by local interneurons dominate the thalamic circuits that process signals traveling from the eye downstream. The anatomical and physiological differences between interneurons and the (relay) cells that project to cortex are vast. To explore how these differences might influence visual processing, we made intracellular recordings from both classes of cells *in vivo*. Macroscopically, all receptive fields were similar, made of two concentrically arranged subregions in which dark and bright stimuli elicited responses of the reverse sign. Microscopically, however, the responses of the two types of cells had opposite profiles. Excitatory stimuli drove trains of single EPSPs in relay cells but graded depolarizations in interneurons. By contrast, suppressive stimuli evoked smooth hyperpolarizations in relay cells but unitary IPSPs in interneurons. Computational analyses suggested that these complementary patterns of response help preserve information encoded within the fine timing of retinal spikes and increase the amount of information transmitted to cortex.

Inhibitory neurons dominate the intrinsic circuits of the lateral geniculate nucleus of the thalamus. Specifically, the neurons that project to cortex, relay cells, rarely form local contacts [1]; rather, most intranuclear connections derive from local interneurons [2, 3]. Even the earliest recordings from relay cells emphasized that inhibition seemed stronger in thalamus than in retina [4]. The inhibition is powerful; it can determine whether relay cells fire tonically or in bursts [5, 6], sharpen visual selectivity [4] and otherwise influence input to cortex. Yet, there is scant knowledge of how thalamic inhibitory circuits operate during vision. By

Author for Correspondence: Judith A. Hirsch 328 Hedco Neurosciences Building, MC 2520 Department of Biological Sciences University of Southern California 3641 Watt Way Los Angeles, CA 90089-2520 jhirsch@usc.edu Voice: 213-821-2210.

*current address: Computational Neurobiology Laboratory, The Salk Institute for Biological Sciences, 10010 N. Torrey Pines Road, La Jolla, CA 92037, USA

Author Contributions: X. Wang and J. A. Hirsch performed the experiments with help from V. Vaingankar and C. Soto Sanchez. X. Wang, J. A. Hirsch and F. T. Sommer contributed to various analyses and X. Wang and F. T. Sommer developed the simulations. X. Wang, J. A. Hirsch and F. T. Sommer wrote the manuscript and X. Wang prepared all figures. Supported by National Institutes of Health EY09593 (J.A.H), the Redwood Center for Theoretical Neuroscience (F.T.S) and the National Science Foundation IIS–0713657 (F.T.S.)

combining whole-cell recording and labeling *in vivo* with visual stimulation and computational analyses, we have been able to explore how local interneurons process sensory information.

Relay cells have receptive fields that comprise a concentric center and surround [4] with push-pull responses to stimuli of the opposite contrast — e.g. where bright stimuli excite, dark inhibit [5, 7]. This arrangement can be explained by a circuit in which retinal cells supply direct excitation via monosynaptic connections and indirect inhibition through local interneurons [2, 8]. Accordingly, our results show that interneurons have receptive fields with a center-surround organization and even have push-pull responses. Also, the responses of interneurons, like relay cells [9], can be approximated with simple computational models. Thus, one might assume that all thalamic receptive fields are built the same way, as appears to be the case for excitatory and inhibitory cells in visual cortex [10, 11].

Steadily accumulating evidence, however, suggests that thalamic relay cells and interneurons have profoundly different anatomical and physiological attributes. For example, ganglion cells synapse with the proximal dendrites of relay cells but favor the distal processes of interneurons [8], where active currents help boost excitation [12]. Further, relay cells communicate through conventional axonal contacts, whereas both dendrites and axons of local interneurons form synapses with target cells [8, 13].

Our results showed that these differences between cell types were reflected by dramatically distinct visual responses. For relay cells, preferred stimuli evoked large, unitary excitatory postsynaptic potentials (EPSPs) whereas non-preferred stimuli elicited graded inhibition. The picture for interneurons was the inverse; excitation was smooth while inhibitory responses comprised jagged trains of unitary inhibitory postsynaptic potentials (IPSPs). The rates and receptive field of both types of unitary events were consistent with a feedforward origin.

The difference between signals could, in principle, be explained by differences in anatomical connectivity [8, 13-16] and membrane properties [12, 17]. Moreover, computational and theoretical analyses suggested that the inverted forms of excitation and inhibition work in concert to transmit precise temporal information from the periphery to cortex. Since much of the structure of thalamic circuits is conserved across species and modalities [14, 18], it is likely that our results illustrate a fundamental property of sensory processing.

RESULTS

We made whole-cell recordings from 119 cells in 22 adult female cats, 1.5–4.5 kg and sampled the main layers, A, A1 and C, of the lateral geniculate. We were able to stain 36 neurons, including 27 relay cells and 9 interneurons [19-21]. These and remaining cells were also classified by physiological criteria we discuss below.

Distribution of excitation and inhibition in the receptive field

The most basic question we asked was if the receptive fields of interneurons resembled those of relay cells (**Fig. 1a–f**). Relay cells have receptive fields made of a center and

surround in which stimuli of the reverse contrast evoke responses of the opposite sign [5]. Dark disks flashed in the center of an OFF (X–type) relay cell (**Fig. 1a**) drove excitatory responses (**Fig. 1c**, top) whereas bright disks evoked hyperpolarization (**Fig. 1c**, bottom) as illustrated by averaged records of the membrane voltage following repeated trials of the stimulus. The equivalent situation held for responses to annuli flashed in the surround (**Fig. 1e**). The excitation, or push, is almost certainly fed forward from retinal ganglion cells of the same center sign [22, 23]. A simple explanation for the pull is that it comes from interneurons that also have receptive fields with a center-surround structure but have the opposite preference for stimulus contrast (Supplementary (**Fig. 1a**) and see [5] for evidence that the hyperpolarization results from synaptic inhibition rather than the withdrawal of excitatory drive).

Consistent with this scheme, we found that interneurons had receptive fields with a center-surround structure (**Fig. 1d, f**), as illustrated for ON interneuron (**Fig. 1b**). Moreover, there was a push-pull arrangement of responses in each subregion; bright stimuli in the ON center or dark stimuli in OFF surround were excitatory whereas stimuli of the opposite contrast were inhibitory (**Fig. 1d, f**). Note, the excitatory response of this particular interneuron rose more slowly than that of the relay cell; however this might not indicate a trend for the population (see **Fig. 2**).

Quantitative assessments of receptive fields

Disks and annuli drive the center and surround strongly; they are useful for visualizing spatially opponent excitation and inhibition. The next step was to compare the synaptic responses of relay cells and interneurons quantitatively at higher spatial resolution. For this analysis we used Gaussian white noise [24].

Past studies of relay cells have employed simple linear-nonlinear models to characterize neural responses [24]; we extended this approach to interneurons. We used reverse correlation of synaptic responses to the stimulus to generate spatiotemporal receptive fields shown as contour plots (**Fig. 2a**) alongside the time course for the peak pixel for 4 cells (**Fig. 2b**), an ON and OFF relay cell and an ON and OFF interneuron (note, Gaussian noise lacks spatial coherence and high contrasts and so drove far stronger responses from the center than the surround). The spatial and temporal components of the response were similar for all cell types.

Next we built standard linear-nonlinear cascade models. The linear stage was the response-triggered average of the stimulus (effectively, the receptive field) for which we substituted averages of the membrane current for the conventional spike rate. The second stage was a nonlinearity that mapped the output of the linear filter to the strength of response [24]; the nonlinearity was fit with a sigmoidal function (**Fig. 2c**), though a linear fit performed almost as well. We streamed a novel noise sequence (different from that used for the model) through the model and plotted the result against the actual prerecorded response to the novel stimulus (**Fig. 2d**). The model predicted the responses of all cells to the same extent, as measured by explained variance (**Fig. 2e**). Thus, to a first approximation, the synaptic receptive fields of both relay cells and interneurons appear to be similar in shape and

explanatory power. Note that the explained variance here (roughly 40%) was less than that achieved by past extracellular studies. This is likely because intracellular signals have far more complicated, effectively “noisier”, shapes than spikes and also because we used a long stimulus sequence [5], which precluded presentation of multiple repeats. Similarly, we could not characterize other aspects of the response, such as the contrast gain, to furnish additional parameters for better fits [25]. All told, responses to disks and annuli and to dense noise suggested that the receptive fields of relay cells and interneurons were similar.

Correlating intracellular waveform with cell class

So far, we have described averaged responses to visual stimuli. We next analyzed the intracellular records at a finer grain to learn how receptive fields are built. Taken together, our results showed that relay cells and interneurons processed feedforward drive in stereotypically different ways.

We investigated the structure of neural responses by recording during the presentation of various types of visual stimuli. We used voltage-clamp rather than current-clamp mode to reduce the influence of intrinsic membrane conductances on synaptic input [5]. The membrane currents recorded from most cells (~75%) were dominated by trains of prominent excitatory postsynaptic currents (EPSCs) (**Fig. 3a**) and see [5, 26]. We anatomically identified 27/89 neurons from which recordings were made; all were relay cells including X, Y and W subclasses [5, 26]. This observation was not surprising since retinal inputs produce prominent EPSPs [27](by contrast, events generated by corticothalamic neurons are typically invisible unless the membrane resistance is increased with drugs [28]).

The recordings obtained from the remaining cells (~25%) were strikingly different. The most salient components were brief, net hyperpolarizing currents that were often preceded by depolarizing transients from which the occasional spike escaped (**Fig. 3b**). We labeled 9/30 cells with this physiological profile and found that all were interneurons. Thus, there was a striking qualitative distinction between the two waveforms; one was characterized by unitary depolarizing currents and the other by unitary hyperpolarizing currents. This difference held true for stimuli as diverse as Gaussian noise and natural movies [5, 26].

To quantify the difference between the waveforms, we devised a metric called the “deflection index” (see **Methods** and Supplementary **Fig. 4**). It measured the asymmetry in the inward versus outward deflections of the membrane current over different timescales. The values of the index were positive when the membrane trajectory was hyperpolarizing and were negative for depolarizing excursions. Plots made by measuring the value of the index from short to long intervals for single cells (**Fig. 3c**) confirmed the impression made by eye (see **Fig. 3a, b**). The curves for the (labeled and putative) interneurons peaked at a positive value and those for the (labeled and putative) relay cells peaked at a negative value. Next, we used principal component analysis to characterize the structure of these curves and found that data divided into two separate modes ((**Fig. 3d**). Further, statistical calculations of conditional probability showed that the physiological profile predicted anatomical class with high fidelity (see **METHODS**).

Voltage dependence of membrane currents

It seemed unlikely that the disparity between waveforms merely reflected levels of membrane polarization. Our recordings (**Figs. 1** and **3**) were usually made at holding levels above the reversal for inhibition and just below the threshold for firing in order to visualize excitatory and inhibitory input (and see **Fig. 1** in [5]). Further, one class of response never switched to the other. Also, we usually recorded both types of responses in a single animal (19/22), sometimes one immediately after the other, suggesting the difference in response did not correlate with particular animals or physiological state.

To assess the voltage dependence of the intracellular waveforms, we made recordings from single cells while injecting different amounts of depolarizing and hyperpolarizing current. As anticipated for EPSPs, the inputs recorded from the majority population (labeled and putative relay cells) grew larger as the membrane was made more hyperpolarized (**Fig. 4a**). By contrast, the unitary events recorded from the minority population (labeled and putative interneurons) reversed sign when the membrane was made progressively negative, as expected for events dominated by IPSPs (**Fig. 4b**). Averaged event amplitude with respect to the sign and strength of current injected are illustrated graphically for 3 examples of each cell type (**Fig. 4c**). Thus, the disparity between the shapes of the unitary events seemed to reflect different types of synaptic input.

From the analyses above (**Figs. 3** and **4**), we concluded that relay cells and interneurons can be classified based on synaptic response. From now on, we refer to cells with intracellular currents dominated by EPSCs as relay cells and those with records dominated by IPSCs as interneurons.

Are there other physiological characteristics that distinguish relay cells from interneurons? Previous work *in vitro* showed that interneurons often have thinner action potentials than relay cells [29] but that the distribution of widths overlap [29]. We did not attempt to measure spike width at half height since the high frequency components of the intracellular signals were often filtered, see[10]. Likewise, the general shape of bursts fired at anode break seem different for feline relay cells and interneurons [29],but perhaps too variable for quantitative comparison.

Visual modulation of different types of synaptic inputs

How do the different patterns of synaptic input we have illustrated (**Figs. 3** and **4**) sum to create the push-pull responses depicted as averages (**Fig. 1**)? To address this question we analyzed individual responses to dark and bright disks. For relay cells, the push (excitation) was made from trains of EPSCs. This pattern is illustrated by responses of an OFF cell to dark disks, shown as two trials of the stimulus in black with the average of all trials in a lighter shade (**Fig. 5a**, top). By contrast, the pull (inhibition) evoked by bright disks was graded (**Fig. 5a**, bottom). The situation for the interneurons was inverted. The push was so smooth that depolarizing synaptic events could not be resolved (**Fig. 5b**, top). By contrast, the pull was made by rapid trains of inhibitory events (**Fig. 5b**, bottom). To view examples of individual responses in current-clamp mode see (Supplementary **Fig. 3**).

The receptive fields of all the unitary excitatory and inhibitory events had a center-surround structure, as if driven by retinal afferents. We asked if the unitary events shared another feature with ganglion cells, sustained fast rates [30, 31] (corticothalamic neurons have slow rates [32]). Thus, we detected unitary events before, during and after the disks were flashed in the center of the receptive fields (see **METHODS**). Sample traces of membrane currents recorded from a single relay cell and interneuron are shown above histograms of event counts (EPSCs for relay cells and IPSCs for interneurons) from five different cells of each type (**Fig. 6**). Responses to disks of the preferred contrast are shown at left (**Fig. 6a, c**) and to the non-preferred contrast at right (**Fig.6b, d**). The range in sustained event rates (measured during the second half of the stimulus interval) for excitatory stimuli was 34.2 – 76.9 (54.5 ± 17.3, mean ± standard deviation) event/s for interneurons and 40.3 – 184.3 (112.2 ± 65.5) event/s for relay cells. The range for suppressive stimuli was 0.8 — 9.2 (4.1 ± 3.8) event/s for interneurons and 0.0 – 38.2 (8.2 ± 16.8) event/s for relay cells.

The event rates for some relay cells (e.g. black traces (**Fig. 6a, b**) were faster than those for others and all interneurons. These higher rates likely represent convergent retinal input [22, 23, 33]. Accordingly, an expanded segment of the trace (**Fig. 6b**, inset) revealed large and small EPSCs that were probably generated by more than one ganglion cell. The results of this analysis suggested that both types of unitary events track retinal input.

Distribution of receptive fields in visual space

Anatomical studies shows that relay cells and interneurons populate the full extent of the lateral geniculate [2, 3, 34]. Thus, one would expect that the two types of responses should appear at all retinotopic positions. We assessed the distribution of the receptive fields of both types of cells across visual space by marking their positions (relative to the area centralis) on a tangent screen.

The range of occurrence for relay cells (**Fig. 7a, b**) and interneurons (**Fig. 7c, d**) were similar and covered most of the geniculate. The inferior and superior locations that seem undersampled correspond to only small slivers of tissue. Thus, the two types of processing we describe were a ubiquitous feature of the nucleus.

Modeling different patterns of synaptic integration

We used an exponential leaky integrate-and-fire model to explore how the distinct forms of synaptic integration we have described might influence the quality and quantity of information that relay cells transmit downstream. The parameters of the model were based on intracellular recordings from relay cells [35, 36] and on evidence that most relay cells receive input from a single, dominant retinal input (e.g. [23]) and multiple interneurons (e.g. [37]). The signal that drove the model had statistics based on natural scenes (pink noise) and was mediated by excitatory (AMPA) and inhibitory ($GABA_A$) conductances driven in a push-pull pattern.

We compared the results of three different versions of the model, using information theory to quantify how efficiently the sensory signal was encoded by the relay cell's spike train (**Fig. 8**). The control model simulated the actual pattern of jagged excitation and smooth

inhibition we recorded from relay cells, (**Fig. 8b, c**, top, black). For the remaining two models, we altered the pattern of synaptic response either by smoothing excitation (**Fig. 8b, c**, middle, green) or by using jagged inhibition (**Fig. 8b, c**, bottom, purple)(see **METHODS)**.

The first question we asked was how each different condition influenced the transmission of information across varied timescales. Our simulations showed that the effect of smoothing excitation was to reduce the information rate density in the millisecond range (**Fig. 8d**); that is, this quantity grew more slowly as spike times were measured with progressively greater temporal precision. The total amount of information conveyed per unit time at fine time scales was reduced as well (**Fig. 8e**). Altering inhibition by replacing smooth with jagged IPSCs also had a deleterious effect. This manipulation decreased the information transmitted across time scales (**Fig. 8e**) because it corrupted temporal relationships between retinal inputs and the spikes they evoked from relay cells. Next we estimated the total rate of information the relay cell transmitted in each of the three cases. The control simulations yielded significantly higher rates than either test case (**Fig. 8f**). All told, the results of our simulations suggested that jagged excitation was important for relaying temporally precise information whereas smooth inhibition improved the transfer of information overall.

DISCUSSION

Our study provided the first intracellular analysis of how local interneurons in the lateral geniculate nucleus of the thalamus encode visual stimuli. Studies of relay cells had shown that ON and OFF stimuli flashed in the center or surround of the receptive field evoke responses of the opposite sign[5]. This push-pull pattern is most easily explained by direct excitation from the retina and indirect inhibition routed through local interneurons (Supplementary **Fig.1a**). Consistent with this scheme, we found that receptive fields of local interneurons resembled those of relay cells. Despite this similarity, the synaptic inputs recorded from the two types of cells during visual stimulation had almost inverted shapes. Excitatory stimuli evoked rapid sequences of unitary excitatory events in relay cells but relatively smooth and graded depolarizations in interneurons. By contrast, suppressive stimuli elicited smooth and graded inhibition in relay cells but rapid trains of unitary inhibitory events in interneurons. The rates and receptive fields of both types of unitary events appeared to be inherited, directly or indirectly, from retinal ganglion cells. Thus, the high-frequency components of afferent activity were retained in the excitatory responses of relay cells but low-pass filtered in the inhibitory responses; and vice versa for interneurons. Simulations based on our recordings suggest that these different patterns of response work together to preserve the fine temporal structure of retinal activity and transmit information effectively.

Differences between relay cells and interneurons

The membrane currents recorded from the lateral geniculate divided into two different types of waveforms. This dichotomy did not reflect somatic versus dendritic recording sites since electrode tracks confirmed that patches were made at or near the soma. Nor did the divide correlate with presence or absence of triads; records from all relay cells were similar (triads

involve synaptically coupled dendrites of two cells, an interneuron and either a relay cell (commonly X-type) or a second interneuron, that are innervated by a single retinal bouton [8, 13, 38]). Rather, the disparities in waveform correlated with relay cells versus interneurons.

Receptive field structure of interneurons

Earlier extracellular studies of the thalamus suggest that all cells in the main layers of the geniculate have receptive fields with a center-surround structure [20, 21, 33, 39, 40]. Our analyses moved beyond these early studies in two essential ways. First, we were often able to stain cells and link receptive field structure with morphological class. Second, since intracellular recording gives view of subthreshold inputs, we were able to show that interneurons and relay cells alike had a push-pull arrangement of excitation and inhibition within the center and the surround.

Push-pull in a single neuron extends the dynamic range of operation and speeds responses to reversals in stimulus polarity. These effects might be amplified when presynaptic cells also have push-pull responses. For example, interneurons would alternately inhibit or disinhibit their targets as luminance contrast changes from the non-preferred to the preferred. The presence of push-pull is also seen in retina and in (the cat's) cortical layer 4 [7, 11]; hence, it appears to be a basic principle for constructing neural circuits in the early visual pathway.

We do not wish to give the impression that responses of interneurons and relay cells will prove to be identical. For example, the two types of cells might differ in adaptation to contrast and/or luminance [25]. Also, since interneurons receive many more retinal synapses than relay cells [2, 3], they might have larger receptive fields; our current sample is too small to address this issue. Further, since we did not recover labeled cells in the interlamainar zones, we doubt that we recorded there.

Patterns of synaptic input that build receptive fields

Before we began this series of experiments, it seemed likely that relay cells and interneurons were wired in similar ways. This idea was based, in part, on our past studies of the input layer of the cat’ s cortex, which showed that excitatory and inhibitory cells not only had indistinguishable receptive fields but also seemed to use similar patterns of synaptic integration[10, 11]. That is, in cortex, it was impossible to discriminate one type of cell from the other based on subthreshold patterns of response. However, our current results suggested that thalamic relay cells and interneurons build their receptive fields using different synaptic mechanisms. How might these differences arise?

The unitary synaptic inputs that provide the main excitatory drive, or push, to relay cells almost certainly derive from retina. These inputs have the prominent size and stereotyped shapes of retinogeniculate EPSPs [5, 26, 36] and also preserve the fast rates and receptive field structure of ganglion cells [30, 31]. Why, then, should unitary retinal inputs to interneurons be difficult to detect *in vivo*? Cable models show that retinal inputs to interneurons are often electrotonically remote and thus might attenuate before reaching the soma if dendrites were passive [41]. However, recent work shows that retinal input activates dendritic L-type calcium

currents that prevent attenuation by propagating excitation over long distances[12]. Thus, either proximal or distal retinal inputs might be masked by the intrinsic conductances they evoke [12]. In addition, summation of multiple retinal inputs [2, 3, 12] as well as metabotropic components of the synapse [17] could further smooth the time course of feedforward drive. Last, local collaterals of relay cells might supplement retinal inputs [1, 42, 43] by providing disynaptic feedforward excitation.

For relay cells, we hypothesize that the pull, or inhibitory response to stimuli of the opposite contrast, derives from local interneurons whose pooled input [8] averages to generate a graded signal, perhaps with a contribution from the perigeniculate nucleus[44]. Local interneurons also have strong pull responses, but these are built by serial hyperpolarizing deflections that have the fast maintained rates typical of ganglion cells [30, 31]. A brief depolarizing notch often preceded each deflection, indicating an excitatory component. We can only speculate about the underlying circuitry. Here we outline one idea that takes the rate and shape of the deflections into account and is consistent with ultrastructural evidence that shows that interneurons not only receive substantial input from the retina [2, 3] but also form dendrodendritic synapses with each other [14, 45]. We illustrate this idea using an ON interneuron whose push is generated by presynaptic ON ganglion cells. This ON interneuron receives additional retinal input from an OFF ganglion cell that also synapses with a dendrite of an OFF interneuron. Further, the ON interneuron is postsynaptic to the dendrite of that OFF interneuron. Each time the OFF ganglion cell fired, it would produce a monosynaptic EPSC in the ON interneuron that would be cut short by a disynaptic IPSC fed forward from the OFF interneuron. This sequence of events would produce an event like that we observe, Supplementary (**Fig. 1b**).

Of course other patterns of connectivity could build the pull in interneurons. The notches that precede IPSCs might come from strong intrinsic repolarizing currents [46], dendritic spikelets [47] or electrically coupled cells [48]. The IPSCs might be generated by axonal connections from multiple interneurons or, though unlikely [12, 17], sign-inverting retinal synapses onto interneurons. It is doubtful that the pull comes from neurons the perigeniculate nucleus, however. These cells provide weak if any input to local interneurons [44] and do not have receptive fields with a center-surround structure [39].

Shapes of synaptic inputs and the relay of information

Relay cells fire action potentials that lock to retinal input with millisecond fidelity [23, 26, 39]; presumably, such tight coupling is enabled by the large and discrete shapes of retinogeniculate EPSPs. This temporal precision is important because spike timing is critical for encoding sensory information [26, 49]. Our simulations supported these conclusions by showing that jagged excitation is optimal for conveying information at fine time scales.

Why should the pull signal in interneurons retain the high-frequency component of retinal spike trains? Perhaps the reason is to disinhibit relay cells on the timescale of single EPSPs and so preserve the temporal structure of retinal input.

Several different mechanisms might generate the smooth, or low-passed, profiles we recorded from interneurons and relay cells. The push signal in interneurons is probably

blurred by the regenerative currents [12] engaged by retinal input. This form of synaptic integration might decouple the timings of pre– and postsynaptic spikes. Past work supports this idea. Cross-correlations made from spike trains of simultaneously recorded ganglion cells and putative interneurons are broader than those made for ganglion cells and relay cells [39]. Thus, it is reasonable to hypothesize that convergent inhibitory inputs to a relay cell would arrive asynchronously and average to form a smooth pull signal; dendrodendritic input, if present, might be graded.

What role might this low-passed inhibition serve? Our simulations show that smooth versus jagged inhibition has a greater impact on the postsynaptic relay cell's firing rate and increases the amount of information that each spike carries to cortex.

METHODS

Preparation

Adult female cats (1.5 – 3.5 kg) were prepared as described earlier [5]; anesthesia was induced with propofol and sufentanil (20 mg/kg + 1.5 μg/kg, i.v.) and maintained with propofol and sufentanil (5 μg/kg/hr + 1.5 μg/kg/hr, i.v.). All procedures adhered to the guidelines of the National Institutes of Health and the Institutional Animal Care and Use Committee of the University of Southern California.

Stimulation

Discs and annuli and natural movies were displayed at 19–50 frames per second on a computer monitor (refresh rate 144–160 Hz) by means of a stimulus generator (Vsg2/5 or ViSaGe, Cambridge Research Design, Ltd., Cambridge, UK) as described earlier [5]. We also used two-dimensional Gaussian white noise at 33% contrast with a spatial resolution of 0.5 or 1 degree (luminance values below 0 and above 2 × mean were truncated); one stimulus trial typically included 16384 frames, updated at 48 Hz with a video refresh of 144 Hz.

Recordings

Whole-cell recordings with dye filled pipettes were made with standard techniques [10] except that we often used electrodes with resistances >20 MΩ to improve chances of recording from small cells. Signals were recorded with an Axopatch 200A amplifier (Axon Instruments, Inc., Union City, CA, now Molecular Devices, Sunnyvale, CA), digitized at 10–20 kHz (Power1401 data acquisition system, Cambridge Electronic Design, Ltd., Cambridge, UK) and stored for further analysis. It was often impractical to assign absolute resting voltage as the ratio of access to seal resistance led to a voltage division in the neural signal [11]. Unless otherwise noted all recordings were made above the reversal potential for inhibition and below the threshold for firing. The integrity of the recordings was monitored by responses to current injection.

Anatomical analysis

Following histological processing [10] cells were identified as interneurons (Guillery type III cells [50]) using standard criteria [19-21, 29, 41, 50] such as complicated and often thin dendrites, appendages on distal processes and small somas (see Supplementary **Fig. 2**). Different

classes of relay cells were also distinguished on the basis of various anatomical characteristics, such as somal size, shape of the dendritic arbor and the presence of grape–like appendages on primary dendrites [19, 20]. Some cells were reconstructed in three dimensions using a Neurolucida System (MicroBrightfield, Williston, VT).

Receptive fields and linear-nonlinear models

Standard methods of reverse–correlation [24] were used to compute the spatiotemporal receptive fields except that the continuous membrane current (from which action currents were removed [5]) was substituted for traditional, discrete spike times, as follows. First the stimulus was rewritten as a two dimensional matrix, S, of size $m \times n$ where m was the number of time bins and n the number of pixels in the receptive field. The receptive field was then $k = (S^{\mathrm{T}}S)^{-1}S^{\mathrm{T}}r$, where r was the continuous response signal of size $m \times 1$. If the stimulus is white noise, as in our experiments, its autocorrelation will be identity and the receptive field can be computed simply by reverse correlation $k = S^{\mathrm{T}}r$.

We computed the spatiotemporal receptive fields from first 15/16 (15360 frames) of the Gaussian white noise sequence and used these as the linear component of the model (the remaining 1/16 (1024 frames) was reserved to assess the performance of the model). The time bin, or temporal resolution (20.8 ms) was set by the rate of stimulus update (48 Hz). The static nonlinearity function was estimated by fitting (least–mean–square) the intracellular response to the output of the spatiotemporal receptive field. The shape of the nonlinearity for interneurons and relay cells was captured by a sigmoid function $f(x) = \frac{a}{1+e^{b(x-c)}}$, which takes into account slight saturation and thresholding of the response. When a linear function was substituted for the sigmoid, the prediction of the model was only slightly worse, less than 3%; thus this choice of parameterization did not appreciably influence the performance of the model. Finally, the performance of the model was assessed by cross–validation (using the reserved 1/16 of the data) and quantified as the explained variance in the response that the model predicted (since the data did not contain multiple trials of the same stimulus, the percentage of explained variance was calculated with respect to the total variance in the signal).

Deflection index

In order to capture asymmetric structures in the direction, or sign, of the membrane trajectory across various time scales, we devised an index that reflects the dominance of inward versus outward deflections in the intracellular signal (see Supplementary **Fig. 4 for** a graphical explanation). First, we differentiated the recordings of the membrane current $I(t)$ (from which action currents had been removed, see [5]) at different time scales, τ. The resulting differentiated signals were:

$$i(t;\tau) = \frac{1}{\tau}\left[I\left(t+\frac{\tau}{2}\right) - I\left(t-\frac{\tau}{2}\right)\right]$$

We then formed distributions of the differentiated signals (i.e. the change in membrane current at a given time scale) and computed the deflection indices $\gamma_1(\tau)$ as the skewness of these distributions.

$$\gamma_1(\tau) = m_3(\tau)\,[m_2(\tau)]^{-\frac{3}{2}}$$

Here $m_2(\tau)$ and $m_3(\tau)$ are the second and third central moments of the distribution of $i(t;\ \tau)$. To characterize the asymmetry of deflection across all time scales, we normalized the deflection indices and performed principal component analysis on the normalized index γ' as a function of time scales for the population (n = 119).

Event sorting and counting

Intracellular, voltage-damped recordings were filtered digitally (Gaussian filter, 0.5 ms bandwidth) and then differentiated twice. Potential neural events, spikes and unitary synaptic currents, were detected as concave local minima (zero crossing of the first derivative with a negative second derivative). Neural events were clustered using commercial software (Spike2, Cambridge Electronic Design, Ltd., Cambridge, UK).

Exponential leaky integrate-and-fire model

Time evolution of membrane potential (V_m) and synaptic conductances (g_E and g_I) of the modeled relay cell were defined as follows:

$$C_m\frac{dV_m}{dt} = g_L\Delta_T e^{\frac{V_m - V_T}{\Delta_T}} - g_L(V_m - E_L) - g_E(V_m - E_E) - g_I(V_m - E_I)$$
$$\tau_E\frac{dg_E}{dt} = -g_E$$
$$\tau_I\frac{dg_I}{dt} = -g_I$$

where C_m = 1 μF/cm^2; g_L = 40 μS/cm^2; Δ_T = 2 ms; V_T = −50 mV; E_L = −60 mV; E_E = 0 mV; E_I = −80 mV; τ_E = 1.5 ms; τ_I = 10 ms. The modeled relay cell received input from a single ganglion cell and four inhibitory interneurons. Each retinal spike triggered an increase in synaptic conductance by g_{Em} = 200 μS/cm^2 or g_{Im} = 12.5 μS/cm^2. When the membrane potential reached V_τ = 0 mV, a spike was fired and the membrane potential returned to V_{reset} = −70 mV.

The spike trains of the inputs to the relay cell (i.e. the ganglion cell and interneurons) were modeled as inhomogeneous Poisson processes that encoded a pink noise signal for which the power was scaled to 1/f for frequencies > 0.5 Hz. Instantaneous firing rates were generated by passing the signal through complementary, inverse (push–pull) exponential nonlinearities. Average firing rates for both types of input were 30 spike/s and the mean firing rate for relay cells was near 10 spikes/s, corresponding to 30–40% efficacy. To model smooth excitation, we increased to τ_E = 10 ms and reduced $\bar{g}_E$ proportionately. To model jagged inhibition, we reduced the number of presynaptic from four to only one and scaled $\bar{g}_I$ proportionately. Simulations made with all three models were done using 32768 repeats of trials of duration, T = 20 s, and sampled at 10 kHz .

Information rates for the thalamic spike trains were estimated at different time scales (τ):

$$I(\tau) = \sum_{t=1}^{T/\tau} \frac{\tau}{T} r(t) \log_2 \frac{r(t)}{\bar{r}}$$

where $r(t)$ was the firing rate of the tth time bin and $\bar{r}$ the mean firing rate. Information rate density was then defined as $i(\tau) = -\frac{dI(\tau)}{d\tau}$, which is the sensitivity of information rate with respect to the time scale at which the firing rate was measured. The total information rate was estimated by extrapolating time scale to zero: $I = \lim_{\tau \to 0} I(\tau)$.

Predicting anatomical class based on physiology

We assessed how well the physiological profile recorded from a given neuron predicted its anatomical class, based on the 36 cases ($k = 36$) for which both physiological and anatomical data were available for the same cell. The accuracy of the match between the anatomical and physiological classification of interneurons (I) and relay cells (R) is given by the conditional probabilities $\alpha = p(I_{phys} \mid I_{anat})$ and $\beta = p(R_{phys} \mid R_{anat})$, respectively.

To estimate the significance of our particular result, we made two assumptions, based on the observation that both the anatomical and physiological classifier yielded the same approximate ratio of two cell types (corresponding to the distribution of relay cells and interneurons reported in the literature, see main text). Specifically, we assumed the ratio of interneurons to relay cells is 1:4 and that the conditional probabilities preserved this ratio. For any given β, these assumptions set α to:

$$\alpha = \frac{(1-p)\beta^2 + (2p-1)\beta}{p\beta}$$

The probability of obtaining the experimental results we observed is:

$$P_0 = \alpha^{kp}\beta^{k(1-p)} = \beta^k \left[\frac{(1-p)\beta^2 + (2p-1)\beta}{p}\right]^{kp}$$

By way of example, if the correspondence between both classifiers were perfect, not just for our small sample, but for any sample size, then $\alpha = \beta = 1$ and the probability of obtaining our experimental result would be certain, $P_0 = 1$.

If we assumed that the physiological classifier randomly assigned anatomical type while preserving the 1:4 ratio of interneurons to relay cells, then $\alpha = 1 - \beta = ¼$. In this case, the probability that we would have found the empirically observed perfect correspondence between physiology and anatomy by chance is extremely low, $P_0 = 10^{-9}$.

Next, rather than estimating the probability of arriving at our empirical result by chance (as above), we specifically asked how faithfully the physiological classifier predicts anatomical type. Thus, we set $P_0 = 0.05$ and calculated the corresponding values for the conditional probabilities α and β. The resulting values were $\alpha = 0.88$ and $\beta = 0.95$, indicating that even

conditional probabilities this close to 1 would yield only an insignificant result. Thus, the actual values for α and β must be much larger. In sum, this analysis suggested that the physiology predicted the anatomy with very high fidelity.

Supplementary Material

Refer to Web version on PubMed Central for supplementary material.

Acknowledgments

We are grateful to L. M. Martinez for discussions throughout the project and thank Q. Wang for custom software. J. Provost, S. X. X. Xing, B. Gary, M. Bathen and M. Gerstmar reconstructed labeled cells and M. Gerstmar also assisted with event sorting.

REFERENCES

1. Bickford ME, et al. Synaptic organization of thalamocortical axon collaterals in the perigeniculate nucleus and dorsal lateral geniculate nucleus. J. Comp. Neurol. 2008; 508:264–285. [PubMed: 18314907]
2. Montero VM. A quantitative study of synaptic contacts on interneurons and relay cells of the cat lateral geniculate nucleus. Exp. Brain Res. 1991; 86:257–270. [PubMed: 1756802]
3. Van Horn SC, Erisir A, Sherman SM. Relative distribution of synapses in the A-laminae of the lateral geniculate nucleus of the cat. J. Comp. Neurol. 2000; 416:509–520. [PubMed: 10660881]
4. Hubel DH, Wiesel TN. Integrative action in the cat's lateral geniculate body. J. Physiol. 1961; 155:385–398. [PubMed: 13716436]
5. Wang X, et al. Feedforward excitation and inhibition evoke dual modes of firing in the cat's visual thalamus during naturalistic viewing. Neuron. 2007; 55:465–478. [PubMed: 17678858]
6. Denning KS, Reinagel P. Visual control of burst priming in the anesthetized lateral geniculate nucleus. J. Neurosci. 2005; 25:3531–3538. [PubMed: 15814783]
7. Martinez LM, et al. Receptive field structure varies with layer in the primary visual cortex. Nat. Neurosci. 2005; 8:372–379. [PubMed: 15711543]
8. Hamos JE, Van Horn SC, Raczkowski D, Uhlrich DJ, Sherman SM. Synaptic connectivity of a local circuit neurone in lateral geniculate nucleus of the cat. Nature. 1985; 317:618–621. [PubMed: 4058571]
9. Dan Y, Atick JJ, Reid RC. Efficient coding of natural scenes in the lateral geniculate nucleus: experimental test of a computational theory. J. Neurosci. 1996; 16:3351–3362. [PubMed: 8627371]
10. Hirsch JA, et al. Functionally distinct inhibitory neurons at the first stage of visual cortical processing. Nat. Neurosci. 2003; 6:1300–1308. [PubMed: 14625553]
11. Hirsch JA, Alonso JM, Reid RC, Martinez LM. Synaptic integration in striate cortical simple cells. J. Neurosci. 1998; 18:9517–9528. [PubMed: 9801388]
12. Acuna-Goycolea C, Brenowitz SD, Regehr WG. Active dendritic conductances dynamically regulate GABA release from thalamic interneurons. Neuron. 2008; 57:420–431. [PubMed: 18255034]
13. Guillery RW. A quantitative study of synaptic interconnections in the dorsal lateral geniculate nucleus of the cat. Z Zellforsch Mikrosk Anat. 1969; 96:39–48.
14. Coomes DL, Bickford ME, Schofield BR. GABAergic circuitry in the dorsal division of the cat medial geniculate nucleus. J. Comp. Neurol. 2002; 453:45–56. [PubMed: 12357431]
15. Godwin DW, et al. Ultrastructural localization suggests that retinal and cortical inputs access different metabotropic glutamate receptors in the lateral geniculate nucleus. J. Neurosci. 1996; 16:8181–8192. [PubMed: 8987843]
16. Montero VM. Localization of gamma-aminobutyric acid (GABA) in type 3 cells and demonstration of their source to F2 terminals in the cat lateral geniculate nucleus: a Golgi-

electron- microscopic GABA-immunocytochemical study. J. Comp. Neurol. 1986; 254:228–245. [PubMed: 3540041]

17. Govindaiah G, Cox CL. Metabotropic glutamate receptors differentially regulate GABAergic inhibition in thalamus. J. Neurosci. 2006; 26:13443–13453. [PubMed: 17192427]
18. Wilson JR, Forestner DM, Cramer RP. Quantitative analyses of synaptic contacts of interneurons in the dorsal lateral geniculate nucleus of the squirrel monkey. Vis. Neurosci. 1996; 13:1129–1142. [PubMed: 8961542]
19. Friedlander MJ, Lin CS, Stanford LR, Sherman SM. Morphology of functionally identified neurons in lateral geniculate nucleus of the cat. J. Neurophysiol. 1981; 46:80–129. [PubMed: 7264710]
20. Humphrey AL, Weller RE. Structural correlates of functionally distinct X-cells in the lateral geniculate nucleus of the cat. J. Comp. Neurol. 1988; 268:448–468. [PubMed: 3360998]
21. Sherman SM, Friedlander MJ. Identification of X versus Y properties for interneurons in the A-laminae of the cat's lateral geniculate nucleus. Exp. Brain Res. 1988; 73:384–392. [PubMed: 3215314]
22. Levick WR, Cleland BG, Dubin MW. Lateral geniculate neurons of cat: retinal inputs and physiology. Investigative Ophthalmology. 1972; 11:302–311. [PubMed: 5028229]
23. Usrey WM, Reppas JB, Reid RC. Specificity and strength of retinogeniculate connections. J. Neurophysiol. 1999; 82:3527–3540. [PubMed: 10601479]
24. Schwartz O, Pillow JW, Rust NC, Simoncelli EP. Spike-triggered neural characterization. Journal of Vision. 2006; 6:484–507. [PubMed: 16889482]
25. Mante V, Bonin V, Carandini M. Functional mechanisms shaping lateral geniculate responses to artificial and natural stimuli. Neuron. 2008; 58:625–638. [PubMed: 18498742]
26. Koepsell K, et al. Retinal oscillations carry visual information to cortex. Front. Sys. Neurosci. 2009; 3
27. Blitz DM, Regehr WG. Timing and specificity of feed-forward inhibition within the LGN. Neuron. 2005; 45:917–928. [PubMed: 15797552]
28. Granseth B, Lindstrom S. Unitary EPSCs of corticogeniculate fibers in the rat dorsal lateral geniculate nucleus In vitro. J. Neurophysiol. 2003; 89:2952–2960. [PubMed: 12611977]
29. Pape HC, McCormick DA. Electrophysiological and pharmacological properties of interneurons in the cat dorsal lateral geniculate nucleus. Neuroscience. 1995; 68:1105–1125. [PubMed: 8544986]
30. Frishman LJ, Levine MW. Statistics of the maintained discharge of cat retinal ganglion cells. J. Physiol. 1983; 339:475–494. [PubMed: 6887030]
31. Bullier J, Norton TT. Comparison of receptive-field properties of X and Y ganglion cells with X and Y lateral geniculate cells in the cat. J. Neurophysiol. 1979; 42:274–291. [PubMed: 219159]
32. Gilbert CD. Laminar differences in receptive field properties of cells in cat primary visual cortex. J. Physiol. 1977; 268:391–421. [PubMed: 874916]
33. Mastronarde DN. Nonlagged relay cells and interneurons in the cat lateral geniculate nucleus: receptive-field properties and retinal inputs. Vis. Neurosci. 1992; 8:407–441. [PubMed: 1586644]
34. Fitzpatrick D, Penny GR, Schmechel DE. Glutamic acid decarboxylase-immunoreactive neurons and terminals in the lateral geniculate nucleus of the cat. J. Neurosci. 1984; 4:1809–1829. [PubMed: 6376726]
35. Destexhe A, Neubig M, Ulrich D, Huguenard J. Dendritic low-threshold calcium currents in thalamic relay cells. J. Neurosci. 1998; 18:3574–3588. [PubMed: 9570789]
36. Blitz DM, Regehr WG. Retinogeniculate synaptic properties controlling spike number and timing in relay neurons. J. Neurophysiol. 2003; 90:2438–2450. [PubMed: 14534270]
37. Hirsch JC, Burnod Y. A synaptically evoked late hyperpolarization in the rat dorsolateral geniculate neurons in vitro. Neuroscience. 1987; 23:457–468. [PubMed: 3437975]
38. Datskovskaia A, Carden WB, Bickford ME. Y retinal terminals contact interneurons in the cat dorsal lateral geniculate nucleus. J. Comp. Neurol. 2001; 430:85–100. [PubMed: 11135247]
39. Dubin MW, Cleland BG. Organization of visual inputs to interneurons of lateral geniculate nucleus of the cat. J. Neurophysiol. 1977; 40:410–427. [PubMed: 191574]

40. Wilson J. Synaptic organization of individual neurons in the macaque lateral geniculate nucleus. J. Neurosci. 1989; 9:2931–2953. [PubMed: 2769372]
41. Bloomfield SA, Sherman SM. Dendritic current flow in relay cells and interneurons of the cat's lateral geniculate nucleus. Proc. Natl. Acad. Sci. 1989; 86:3911–3914. [PubMed: 2542955]
42. Cox CL, Reichova I, Sherman SM. Functional synaptic contacts by intranuclear axon collaterals of thalamic relay neurons. J. Neurosci. 2003; 23:7642–7646. [PubMed: 12930803]
43. Lorincz ML, Kekesi KA, Juhasz G, Crunelli V, Hughes SW. Temporal framing of thalamic relay-mode firing by phasic inhibition during the alpha rhythm. Neuron. 2009; 63:683–696. [PubMed: 19755110]
44. Cucchiaro JB, Uhlrich DJ, Sherman SM. Electron-microscopic analysis of synaptic input from the perigeniculate nucleus to the A-laminae of the lateral geniculate nucleus in cats. J. Comp. Neurol. 1991; 310:316–336. [PubMed: 1723987]
45. Pasik P, Pasik T, Hámori J. Synapses between interneurons in the lateral geniculate nucleus of monkeys. Exp. Brain Res. 1976; 25:1–13. [PubMed: 817920]
46. Person AL, Perkel DJ. Unitary IPSPs drive precise thalamic spiking in a circuit required for learning. Neuron. 2005; 46:129–140. [PubMed: 15820699]
47. Contreras D, Curro Dossi R, Steriade M. Electrophysiological properties of cat reticular thalamic neurones in vivo. J. Physiol. 1993; 470:273–294. [PubMed: 8308730]
48. Landisman CE, et al. Electrical synapses in the thalamic reticular nucleus. J. Neurosci. 2002; 22:1002–1009. [PubMed: 11826128]
49. Butts DA, et al. Temporal precision in the neural code and the timescales of natural vision. Nature. 2007; 449:92–95. [PubMed: 17805296]
50. Guillery RW. A study of Golgi preparations from the dorsal lateral geniculate nucleus of the adult cat. J. Comp. Neurol. 1966; 128:21–50. [PubMed: 4165857]

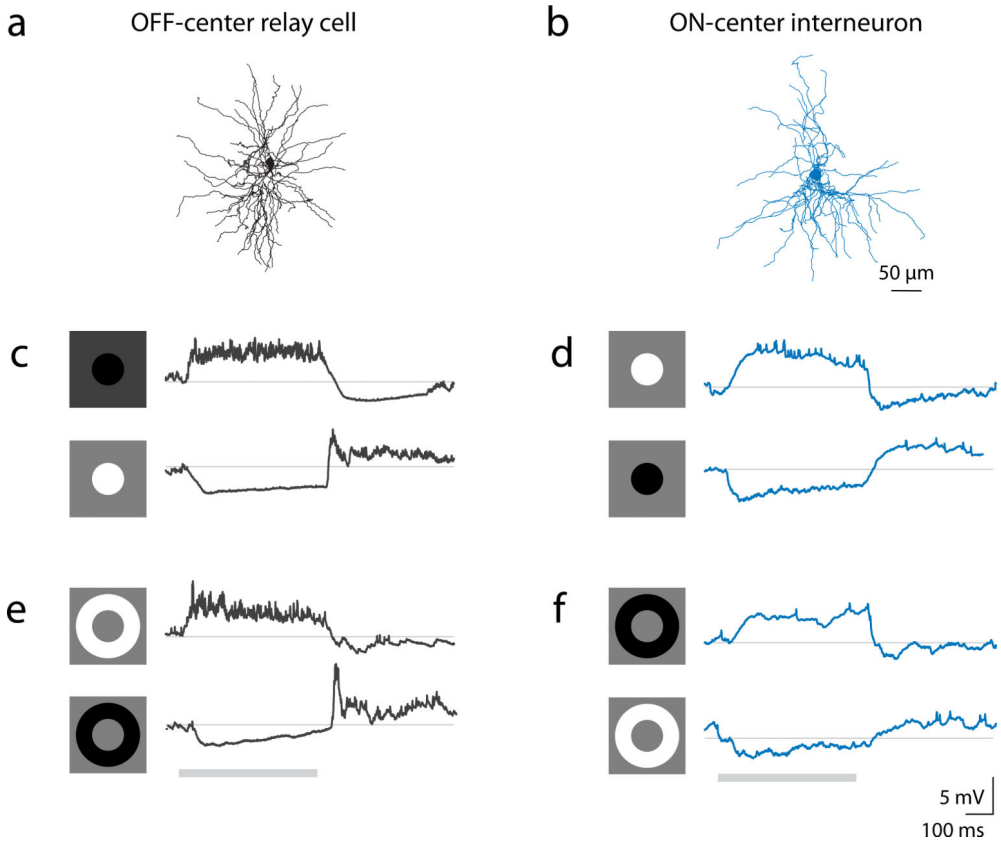

Figure 1. Push-pull responses of an OFF-center relay cell and ON-center interneuron

(**a**) Anatomical reconstruction of an OFF-center relay cell drawn above the averaged responses of the membrane voltage to dark and bright disks flashed in center (**c**) and annuli flashed in the surround (**e**) of the receptive field, black traces The icons at left depict stimulus shape and contrast while the gray line under the traces marks stimulus duration. (**b**) Reconstruction of the dendrites of an ON-center interneuron (the axon was too pale to trace continuously). Responses of the interneuron evoked from the center (**d**) and surround (**f**) of the receptive field, blue traces ; conventions as in (**c, e**). Scale bars are the same for (**a, b**) and (**c – f**).

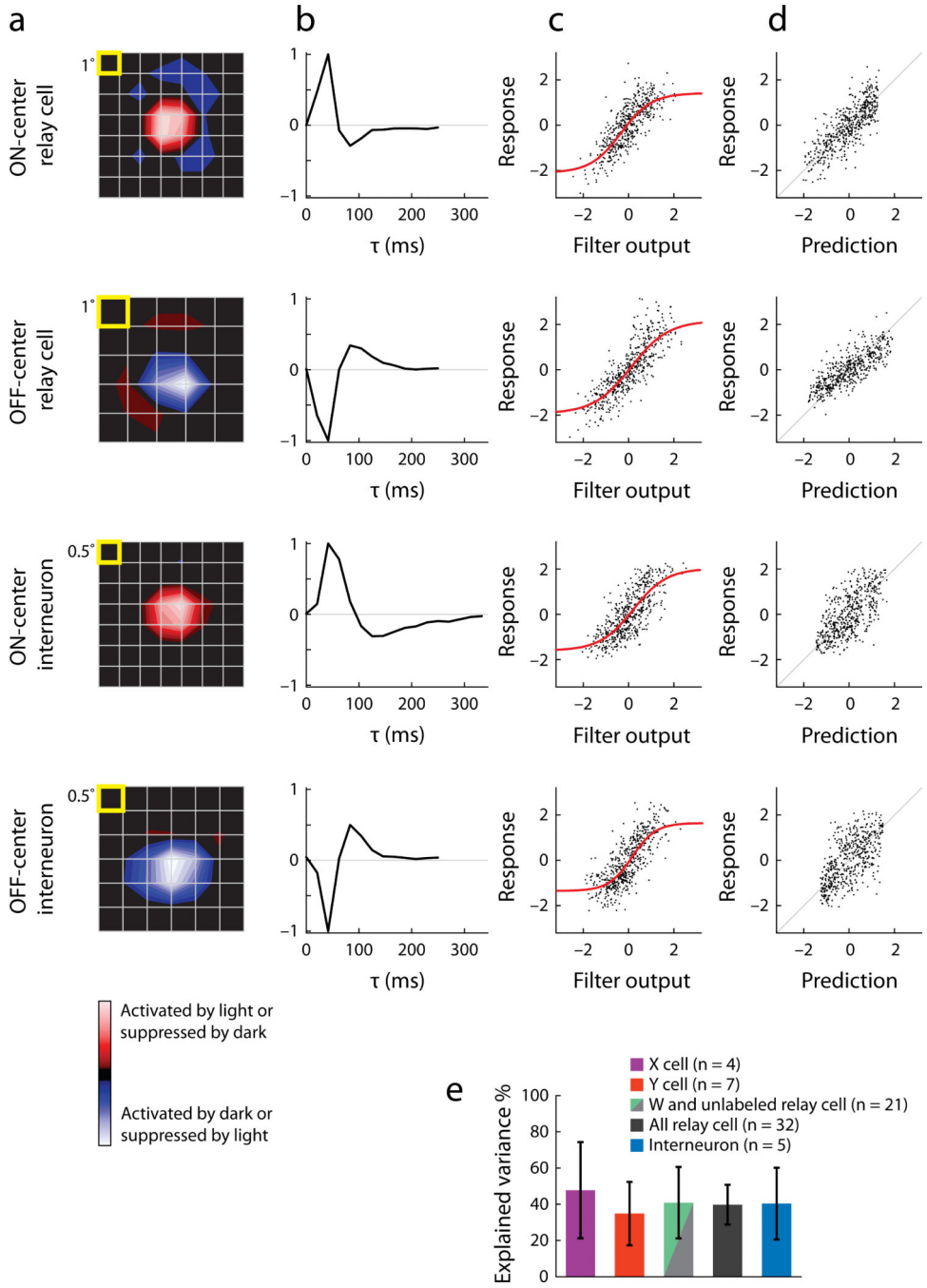

Figure 2. Receptive fields of relay cells and interneurons and prediction of neural responses using linear-nonlinear models

Spatial (**a**) and temporal (**b**) receptive fields of two relay cells and two interneurons computed from the intracellular response (see [5]). Stimulus size is indicated by the yellow box, color codes are explained by the legend at bottom. Scatter plots of the actual intracellular response against that obtained using a linear filter made from the spatiotemporal receptive field show how the nonlinear (red curve) component of the model was fit (**c**). Comparison of the actual and predicted responses (**d**); the actual response was normalized so that the mean was zero and the variance was unity. Performance of the model

(**e**), quantified by explained variance for populations of relay cells (n = 32) and interneurons (n = 5); color codes for the different classes and subclasses of cells are provided in the legend; error bars represent standard deviation.

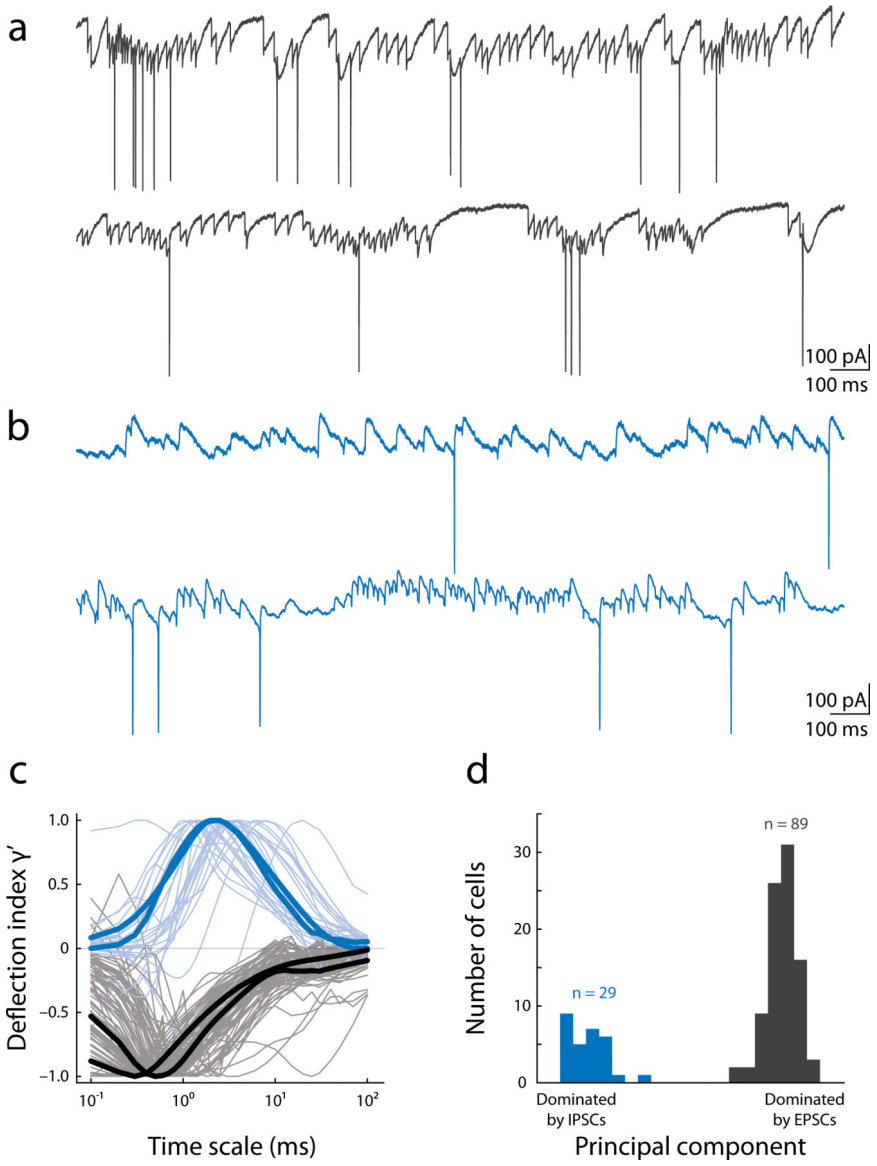

Figure 3. Quantitative comparison of postsynaptic currents recorded from all cells

Examples of membrane currents characteristic of relay cells in black (**a**) and interneurons in blue (**b**) recorded in response to Gaussian noise (**a, b** top) or natural movies (**a, b** bottom) for four different cells. Normalized deflection indices plotted against time scale for the whole dataset (n = 119) (**c**); darker thicker curves are from neurons illustrated in **a, b**. Histogram plotting the distribution of the first principal component of the deflection indices (**d**).

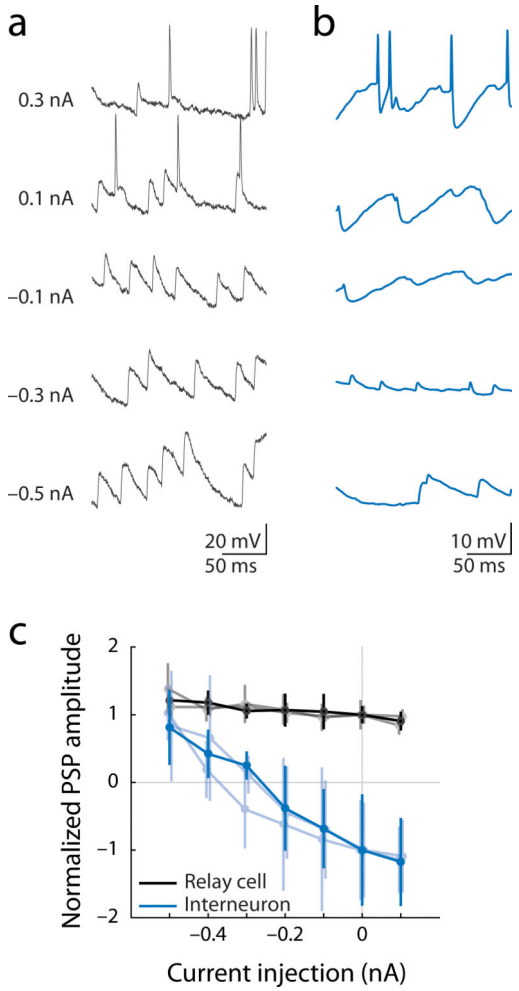

Figure 4. Voltage dependence of postsynaptic potentials recorded from relay cells and interneurons

Spontaneous inputs to a relay cell (**a**) and interneuron (**b**) recorded while different amounts of current were injected, as indicated at left. Amplitudes of PSPs as a function of current injection, normalized to PSP amplitude at rest for 3 relay cells and 3 interneurons; error bars indicate the standard deviation; darker lines indicate responses shown in **a** and **b** (**c**). Records from relay cells are in black and from interneurons in blue.

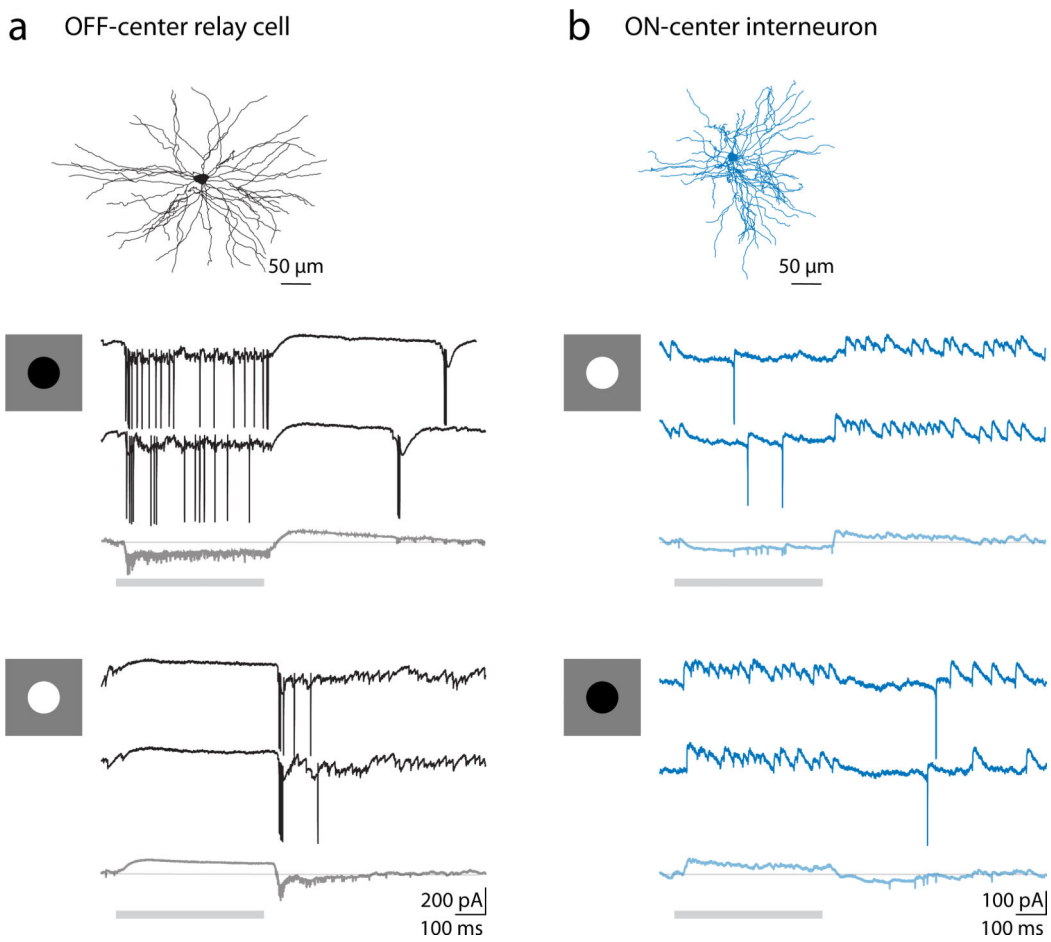

Figure 5. Visual modulation of synaptic inputs to relay cells and interneurons

Responses to disks of the preferred and anti-preferred contrast flashed in the centers of the receptive field of an OFF-center relay cell (**a**, black) and interneuron (**b**, blue). The dendritic arbors of each cell are drawn above responses to two individual presentations of the stimulus (darker colors) and the average for all trials (lighter colors); gray bars indicate stimulus duration.

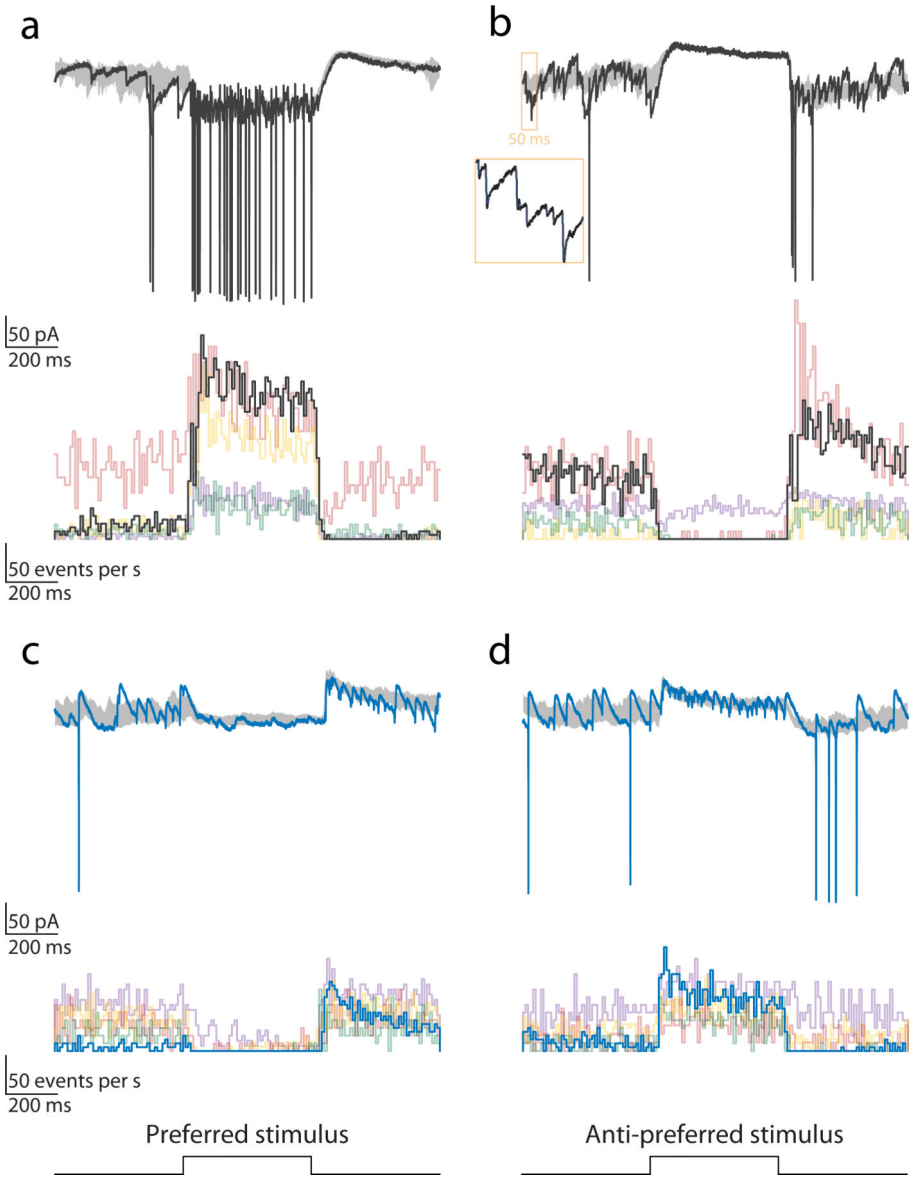

Figure 6. Rates of unitary synaptic events recorded from relay cells and interneurons

Responses to disks of the preferred (**a**) and anti-preferred (**b**) contrast flashed in the center of the receptive field of a relay cell (an example trial, black, and the variance across trials, gray) shown above histograms of EPSC rates for the same (black) and 4 additional relay cells (different colors); bin size is 5ms. Inset shows a segment of the recording at an expanded time scale and doubled gain to reveal differently sized EPSCs. Companion responses and plots of event rate for 5 interneurons (**c, d**).

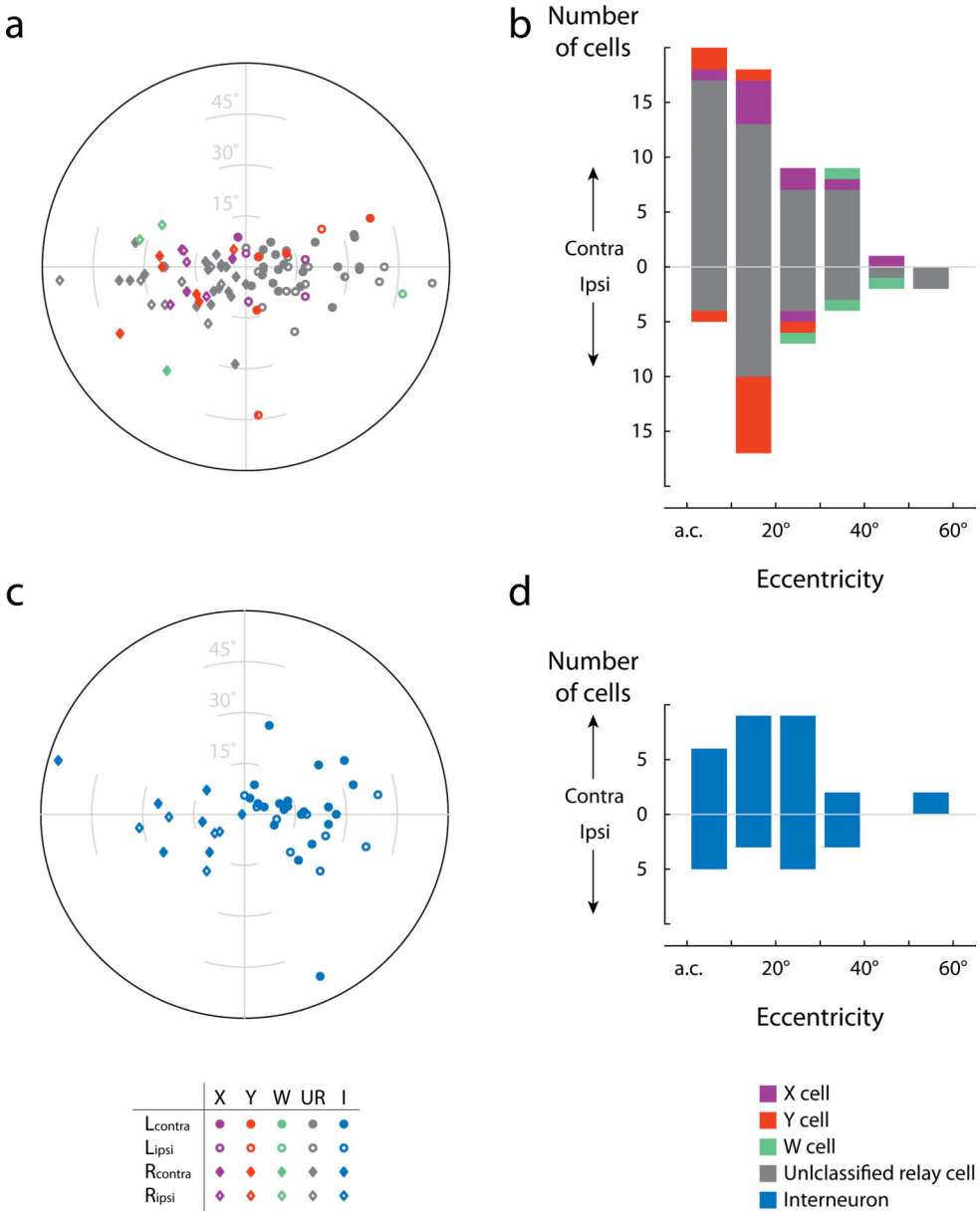

Figure 7. Spatial distribution of relay cells and interneurons

Spatial distribution of the receptive fields of relay cells (**a, b**) and interneurons (**c, d**) shown as polar plots (**a, c**) and frequency histograms (**b, d**). Different types of cells are illustrated with different colors, as indicated in the legend.

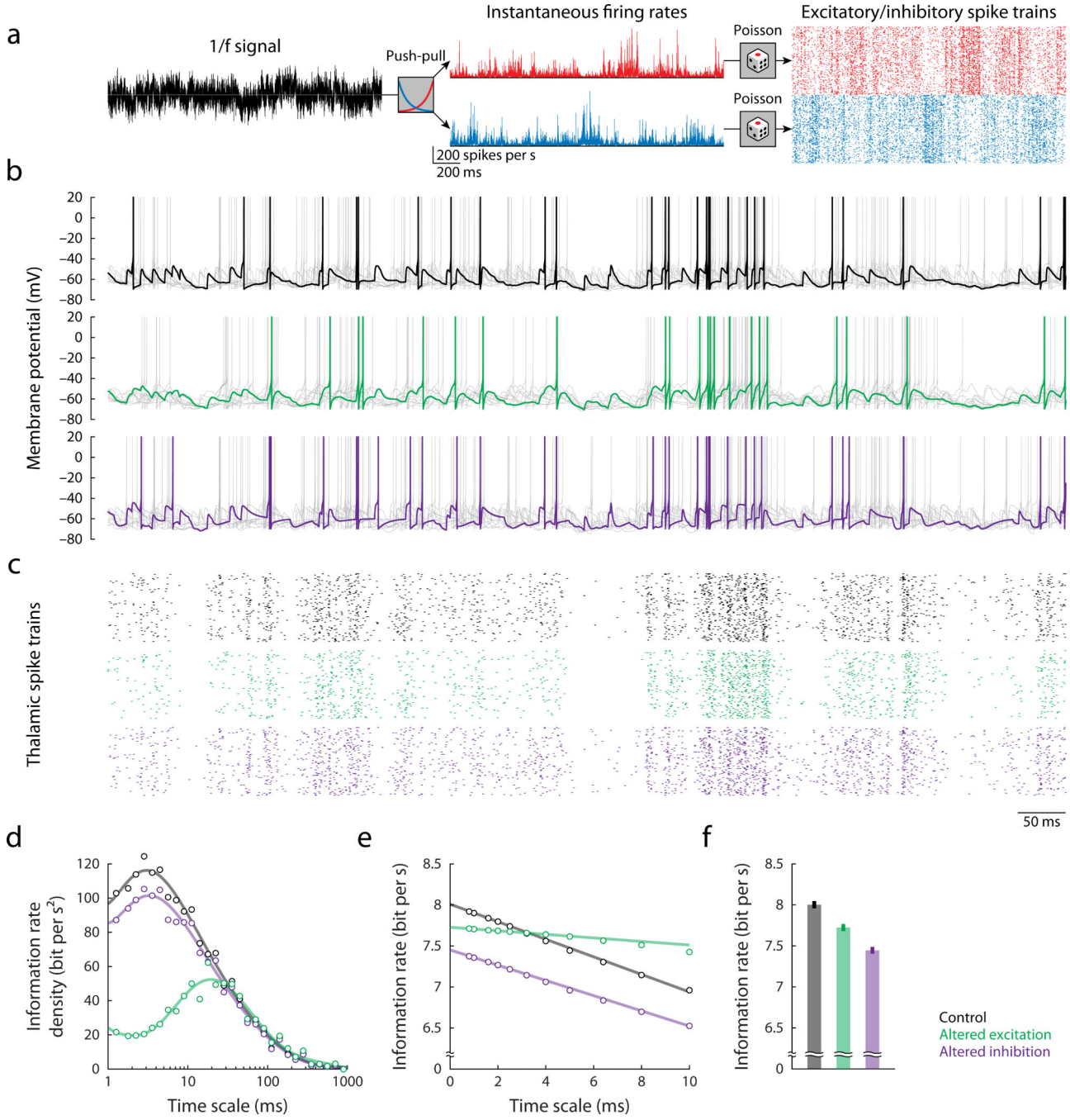

Figure 8. Simulations of information transmitted by circuits that use different forms of synaptic integration

(**a**) Inputs to an exponential leaky integrate-and-fire model of a thalamic relay cell. A pink (1/f) noise signal (left) is transformed by complementary exponential functions to yield antagonistic (push-pull) firing rates (middle) for excitatory (ganglion cell, red) and inhibitory (interneuron, blue) inputs; input spike trains (right, rastergrams showing 100 trials) generated as inhomogeneous Poisson processes. (**b**) Simulated membrane potential for control (black), altered excitation (green) and altered inhibition (purple); dark-colored

traces depict a single trial with 9 additional trials in light gray. (**c**) Rastergrams for 100 trials depict spikes of the modeled relay cell for the three cases. Scale bar applies to (**b**) and (**c**). (**d**) Information rate density plotted as a function of time scale for the three cases; the ordinate represents the negative derivative of the information rate, $i(\tau)$, with respect to τ. (**e**) Estimated information rate for the three cases; error bars in (**f**) represent standard deviations.